

# Ferromagnetic inter-layer coupling in $\text{FeSe}_{1-x}\text{S}_x$ superconductors revealed by inelastic neutron scattering

Mingwei Ma,<sup>1,2,\*</sup> Philippe Bourges,<sup>3</sup> Yvan Sidis,<sup>3</sup> Jinzhao Sun,<sup>2,†</sup> Guoqing Wang,<sup>2</sup> Kazuki Iida,<sup>4</sup> Kazuya Kamazawa,<sup>4</sup> Jitae T. Park,<sup>5</sup> Frederic Bourdarot,<sup>6</sup> Zhian Ren,<sup>1</sup> and Yuan Li<sup>2,7,‡</sup>

<sup>1</sup>*Beijing National Laboratory for Condensed Matter Physics,*

*Institute of Physics, Chinese Academy of Sciences, Beijing 100190, China*

<sup>2</sup>*International Center for Quantum Materials, School of Physics, Peking University, Beijing 100871, China*

<sup>3</sup>*Université Paris-Saclay, CNRS, CEA, Laboratoire Léon Brillouin, 91191, Gif-sur-Yvette, France*

<sup>4</sup>*Neutron Science and Technology Centre, Comprehensive Research Organization for Science and Society (CROSS), Tokai, Ibaraki 319-1106, Japan*

<sup>5</sup>*Heinz Maier-Leibnitz Zentrum (MLZ), Technische Universität München, D-85748 Garching, Germany*

<sup>6</sup>*Université Grenoble Alpes, CEA, IRIG, MEM, MDN, 38000 Grenoble, France*

<sup>7</sup>*Collaborative Innovation Center of Quantum Matter, Beijing 100871, China*

$\text{FeSe}_{1-x}\text{S}_x$  superconductors are commonly considered layered van der Waals materials with negligible inter-layer coupling. Here, using inelastic neutron scattering to study spin excitations in single-crystal samples, we reveal that the magnetic coupling between adjacent Fe layers is not only significant, as it affects excitations up to 15 meV, but also ferromagnetic in nature, making the system different from most unconventional superconductors including iron pnictides. Our observation provides a new standpoint to understand the absence of magnetic order in  $\text{FeSe}_{1-x}\text{S}_x$ . Since intercalating between the Fe layers is known to enhance superconductivity and suppress the inter-layer coupling, superconductivity appears to be a more robust phenomenon in the two-dimensional limit than antiferromagnetic order.

PACS numbers: 74.70.Xa, 78.70.Nx, 74.20.Rp, 74.25.Ha

## I. Introduction

A common thread for understanding unconventional superconductivity is magnetic interactions [1–3], about which inelastic neutron scattering (INS) measurements of spin excitations can provide useful information. Since unconventional superconductors are mostly layered materials, a distinct aspect of such information is the nature and strength of inter-layer magnetic coupling, as manifested by magnetic excitations' momentum dependence along the  $\mathbf{c}^*$  direction.

Taking the well-known spin resonant mode [4] as example, sinusoidal modulation of its intensity along  $\mathbf{c}^*$  in Co/Ni-doped  $\text{BaFe}_2\text{As}_2$  [5–7],  $\text{NaFe}_{0.985}\text{Co}_{0.015}\text{As}$  [8], and  $\text{CeCoIn}_5$  [9], as well as its dispersion in  $\text{BaFe}_2(\text{As}_{1-x}\text{P}_x)_2$  [10], can be attributed to antiferromagnetic spin correlations or interactions between adjacent quintessential layers of atoms that are responsible for both the superconductivity and the magnetism. Such antiferromagnetic coupling is also found in superconductors with two quintessential layers (*i.e.*,  $\text{FeAs}$  or  $\text{Cu}_2\text{O}$  layers) within the primitive cell, such as  $\text{CaKFe}_4\text{As}_4$ ,  $\text{YBa}_2\text{Cu}_3\text{O}_{6+\delta}$  and  $\text{Bi}_2\text{Sr}_2\text{CaCu}_2\text{O}_{8+\delta}$  [11–17]. When the inter-layer coupling is negligible, the spin excitations are observed to be nearly independent of momentum transfer along  $\mathbf{c}^*$ , as found in  $\text{FeSe}_{0.4}\text{Te}_{0.6}$  [18],  $\text{Rb}_x\text{Fe}_{2-y}\text{Se}_2$  [19],  $\text{LaOFeAs}$  [20],  $\text{LiFeAs}$  [21], and  $\text{Li}_{0.8}\text{Fe}_{0.2}\text{ODFeSe}$  [22, 23].

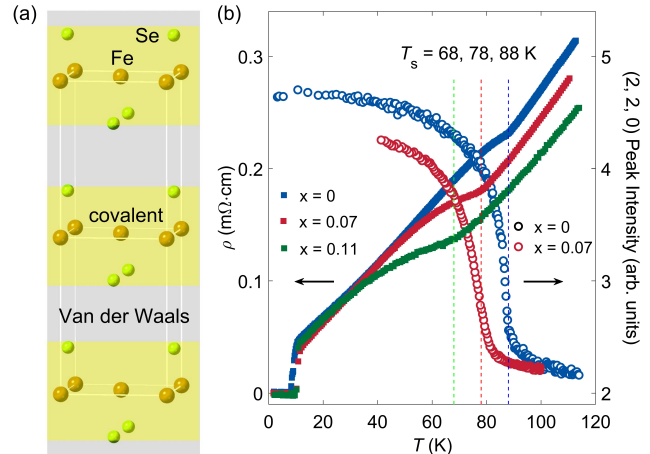


FIG. 1. (a) Crystal structure of FeSe. (b) Temperature dependence of resistivity and intensity of (2, 2, 0) Bragg peak of  $\text{FeSe}_{1-x}\text{S}_x$ . The elastic neutron scattering for measuring (2, 2, 0) Bragg peak were carried on 4F1 spectrometer for FeSe at the Laboratoire Léon Brillouin, Saclay, France and the IN22 spectrometer for  $\text{FeSe}_{0.93}\text{S}_{0.07}$  at the Institut Laue-Langevin, Grenoble, France. They were both mounted in ( $H$ ,  $K$ , 0) scattering plane.

FeSe is regarded as two-dimensional material as it is composed of a stack of strongly bonded edge-sharing  $\text{FeSe}_4$ -tetrahedra layers as shown in Fig. 1(a) [24]. The weak van der Waals bonding between the FeSe

layers allows the material to easily cleave, and it shows potential for use in heterostructure devices with a tunable superconducting transition temperature  $T_c$  above 40 K [25–27]. Additionally, the FeSe layers can be intercalated with different charged or neutral spacer layers, or grown as monolayers on SrTiO<sub>3</sub>, leading to a significant increase of  $T_c$  [28–35].

A unique feature of FeSe is the spontaneous fourfold symmetry breaking observed in the bulk material at the nematic temperature  $T_s = 88$  K, driven by electronic or magnetic instabilities. This nematic state, unlike in Fe-pnictides, does not exhibit long-range magnetic order under ambient pressure [36]. The absence of magnetic order in FeSe has sparked interest from various perspectives, including orbital physics [37] and quantum magnetism such as the spin-fluctuation induced spin-quadrupole order [38], the nematic quantum paramagnetic phase [39], the ferro-orbital order in the nematic phase [40], the near degeneracy between magnetic fluctuations and fluctuations in the charge-current density-wave channel [41] as well as the vertex correction [42].

However, there are few discussions of the absence of magnetic order in FeSe from the viewpoint of the inter-layer coupling. Here we have a try to study its inter-layer coupling revealed by INS and find that the spin resonance mode is highly modulated along  $c$ -axis momentum transfer with maximum at integer  $L = 0, \pm 1, \pm 2$  in an opposite fashion compared to the iron pnictides. Our results suggest a ferromagnetic inter-layer coupling in FeSe.

## II. Experimental methods

The FeSe<sub>1-x</sub>S<sub>x</sub> ( $x = 0, 0.07$  and  $0.11$ ) single crystals have been grown by chemical vapor transport technique [43] and co-aligned with a mosaic within  $5^\circ$  for all the sample arrays as shown in Fig. S1 [See Supplementary Materials]. As displayed in Fig. 1(b) S doping causes a slight increase of  $T_c$  and a substantial decrease of  $T_s$  measured by resistivity and (2, 2, 0) Bragg scattering due to neutron extinction effect [44], and a full suppression is achieved for  $x \geq 0.18$  [45]. Here and throughout this article, the wave vector  $\mathbf{Q}$  is expressed in reciprocal lattice units (r. l. u.) as  $(H, K, L)$ . Using the orthorhombic notation of the 4-Fe Brillouin zone, the wave vector, expressed in inverse Angstrom, is  $\mathbf{Q} = [(2\pi/a)H, (2\pi/a)K, (2\pi/c)L]$  with lattice parameters  $a \approx b \approx 5.32$  Å and  $c \approx 5.52$  Å.

The triple-axis INS experiments with  $k_f = 2.662$  Å<sup>-1</sup> using a focusing pyrolytic graphite (PG) monochromator and analyzer were carried out on the PUMA spectrometer at the Heinz Maier-Leibnitz Zentrum (MLZ),

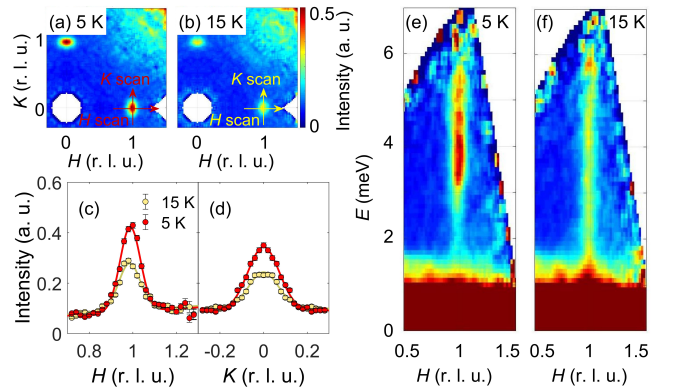


FIG. 2. (a-b) Constant-energy maps of FeSe<sub>0.93</sub>S<sub>0.07</sub> obtained at  $T = 5$  K and  $15$  K in  $(H, K)$  momentum plane with  $|L| \leq 0.2$  and  $E = 4 \pm 1$  meV. (c) Longitudinal scan ( $H$  scan) at  $T = 5$  K and  $15$  K with  $E = 4 \pm 1$  meV,  $|K| \leq 0.1$  and  $|L| \leq 0.2$ . (d) Transverse scan ( $K$  scan) at  $T = 5$  K and  $15$  K with  $E = 4 \pm 1$  meV,  $|H - 1| \leq 0.1$  and  $|L| \leq 0.2$ . (e-f) Energy dependence of two-dimensional slices along  $\mathbf{Q} = (H, 0)$  direction at  $T = 5$  K and  $15$  K with  $|K| \leq 0.1$  and  $|L| \leq 0.2$  for FeSe<sub>0.93</sub>S<sub>0.07</sub>. These data are obtained with incident energy  $E_i = 13.6$  meV on a time of flight spectrometer 4SEASONS. Solid lines in (c-d) are Gaussian functions obtained by fitting the respective data.

Technische Universität München, Garching, Germany, the 2T spectrometer at the Laboratoire Léon Brillouin, Saclay, France and the IN22 spectrometer using the CryoPAD system at the Institut Laue-Langevin, Grenoble, France. Additional PG filters were placed between the sample and the analyzer to eliminate higher-order contaminations. FeSe<sub>1-x</sub>S<sub>x</sub> ( $x = 0, 0.07$  and  $0.11$ ) single crystals were all mounted in the  $(H, 0, L)$  scattering plane.

The time of flight experiments of FeSe<sub>0.93</sub>S<sub>0.07</sub> were performed on the 4SEASONS spectrometer [46] at the Material and Life Science Experimental Facility (MLF), Japan Proton Accelerator Research Complex (J-PARC), Japan. The 4SEASONS spectrometer has a multiple- $E_i$  capability [47, 48] with  $E_i = 10, 13.6, 19.4, 30.1, 52.1$  and  $116$  meV, such that neutron scattering events with a series of different incident energies are recorded simultaneously. During the measurements at  $T = 5$  K,  $15$  K and  $90$  K, the sample was rotated about the vertical direction over a range  $\pm 55^\circ$  and a step  $0.5^\circ$  steps. Data accumulated at different angles were combined into a four-dimensional dataset, in which we used the Horace software packages for reduction and analysis. After a careful alignment of the measured dataset with the crystallographic coordinate system using all available nuclear Bragg reflections, the entire dataset was downfolded into a minimal, physically independent sector of the three-dimensional momentum space using the point-group symmetry of the system.

### III. Results and discussion

Figure 2(a-b) shows the constant-energy maps of spin excitations for  $\text{FeSe}_{0.93}\text{S}_{0.07}$  in the superconducting state ( $T = 5 \text{ K}$ ) and nematic state ( $T = 15 \text{ K}$ ) at  $E = 4 \text{ meV}$  in the  $(H, K)$  plane where the spin excitations are symmetrically located at  $\mathbf{Q} = (\pm 1, 0)$  and  $(0, \pm 1)$  with an elliptic distribution elongated in the transverse direction. The anisotropic distribution can also be displayed by transverse scan ( $K$  scan) and longitudinal scan ( $H$  scan) around  $\mathbf{Q} = (1, 0)$  in Fig. 2(c-d) as indicated by the arrow in Fig. 2(a-b). Compared with the nematic state ( $T = 15 \text{ K}$ ), in superconducting state an enhancement of the spin excitations around  $E \approx 4 \text{ meV}$  is accompanied by a suppression of magnetic response below  $E \approx 2.5 \text{ meV}$  as shown in Fig. 2(e-f), which is a hallmark of the spin resonance mode in agreement with previous INS studies on undoped FeSe [49–53]. The elongated distribution along transverse direction of spin resonance in  $(H, K)$  plane is consistent with the previous work on  $\text{Ba}(\text{Fe}_{0.963}\text{Ni}_{0.037})_2\text{As}_2$  [54],  $\text{CaFe}_{0.88}\text{Co}_{0.12}\text{AsF}$  [55],  $\text{BaFe}_2(\text{As}_{0.7}\text{P}_{0.3})_2$  [56] where the resonance is found to peak sharply at  $\mathbf{Q}_{\text{AF}}$  along the longitudinal direction, but broadens along the transverse direction. Other similar constant-energy maps at  $E = 2\text{--}6 \text{ meV}$  and energy dependence measurements in  $E - K$  space at  $T = 5 \text{ K}$ ,  $15 \text{ K}$  and  $90 \text{ K}$  are displayed in Fig. S2 [See Supplementary Materials]. When entering the tetragonal state ( $T = 90 \text{ K}$ ), the magnetic signals at  $\mathbf{Q} = (\pm 1, 0)$  and  $(0, \pm 1)$  become weak and diffusive on a high background (BG), whereas the scattering signals at  $\mathbf{Q} = (\pm 1, \pm 1)$  are heavily contaminated by  $(1, 1, 0)$  phonon as displayed in Fig. S2(m-r).

After illustrating the anisotropic distribution of spin resonance in  $(H, K)$  plane, we now turn to the  $L$ -modulation of spin resonance. Figure 3(a-b) shows the temperature difference of spin excitations of undoped FeSe and  $\text{FeSe}_{0.93}\text{S}_{0.07}$  between superconducting state ( $T = 2 \text{ K}$ ) and nematic state ( $T = 15 \text{ K}$ ) at  $\mathbf{Q} = (1, 0, L)$  ( $L = 0, 0.5, 1, 1.5$ ). The spin resonance mode appears at  $E_r \approx 3.5 \text{ meV}$  in FeSe, slightly enhanced at  $E_r \approx 4 \text{ meV}$  in  $\text{FeSe}_{0.93}\text{S}_{0.07}$ . Notably, the spin resonance mode presents a stronger intensity at integer  $L = 0$  and  $1$  than that at half-integer  $L$ . This  $L$ -modulation of spin resonance can be further elucidated by the momentum scans along  $\mathbf{Q} = (1, 0, L)$  at  $E = 3.5 \text{ meV}$  for undoped FeSe [Fig. 3(c)] and  $E = 4 \text{ meV}$  for  $\text{FeSe}_{0.93}\text{S}_{0.07}$  [Fig. 3(d)]. In addition, for a higher S doped sample  $\text{FeSe}_{0.89}\text{S}_{0.11}$ , the spin excitations at  $E = 4 \text{ meV}$  in superconducting state are shown in Fig. S5(e) [See Supplementary Materials].

This strongly  $L$ -modulated spin resonance mode in superconducting state is closely related to the anisotropic

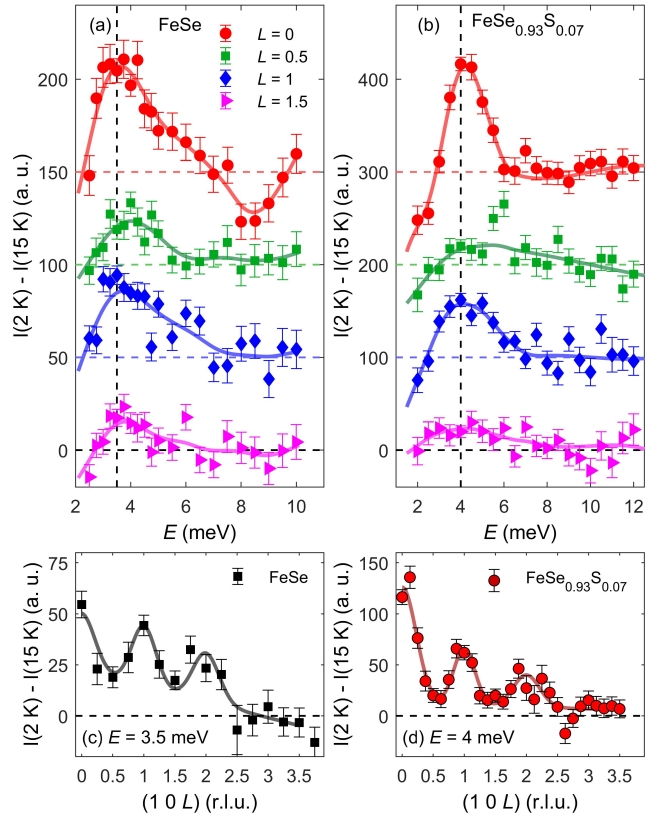


FIG. 3. (a-b) Temperature difference of spin excitations of FeSe and  $\text{FeSe}_{0.93}\text{S}_{0.07}$  between superconducting state ( $T = 2 \text{ K}$ ) and nematic state ( $T = 15 \text{ K}$ ) at  $\mathbf{Q} = (1, 0, L)$  with  $L = 0, 0.5, 1, 1.5$  respectively. (c-d) Temperature difference of spin excitations of FeSe and  $\text{FeSe}_{0.93}\text{S}_{0.07}$  between superconducting state ( $T = 2 \text{ K}$ ) and nematic state ( $T = 15 \text{ K}$ ) along  $L$  direction at  $E = 3.5 \text{ meV}$  and  $4 \text{ meV}$  respectively. Solid lines are the guides to the eyes in (a-b) and multiple Gaussian functions fitted to the respective data in (c-d).

distribution of low-energy spin excitations in momentum space in the nematic state ( $T = 15 \text{ K}$ ). Except for an intensity enhancement due to spin resonance, the anisotropic distribution of spin excitations in momentum space in the nematic state mimics that in superconducting state as displayed in the constant energy maps in  $(H, K)$  plane [Fig. 2(a-b)] and  $(H, L)$  plane [Fig. 4(a-b)] as well as the  $L$  scans in Fig. 4(c). The spin excitations reveal elliptic distribution elongated in the transverse direction and a more elongated ellipse in the  $L$  direction both in superconducting and nematic state. In order to quantitatively clarify the elliptic distribution of spin excitations in three-dimensional momentum space, momentum scans along  $H$ ,  $K$  and  $L$  directions are presented in Fig. 2(c-d), Fig. 4(c) and Fig. S3 [See Supplementary Materials] respectively. The intensity of spin excitations in the nematic state ( $T = 15 \text{ K}$ ) along the longitudinal ( $H$ ), transverse ( $K$ ) and  $L$  directions can be well fitted by Gaussian functions, revealing the full

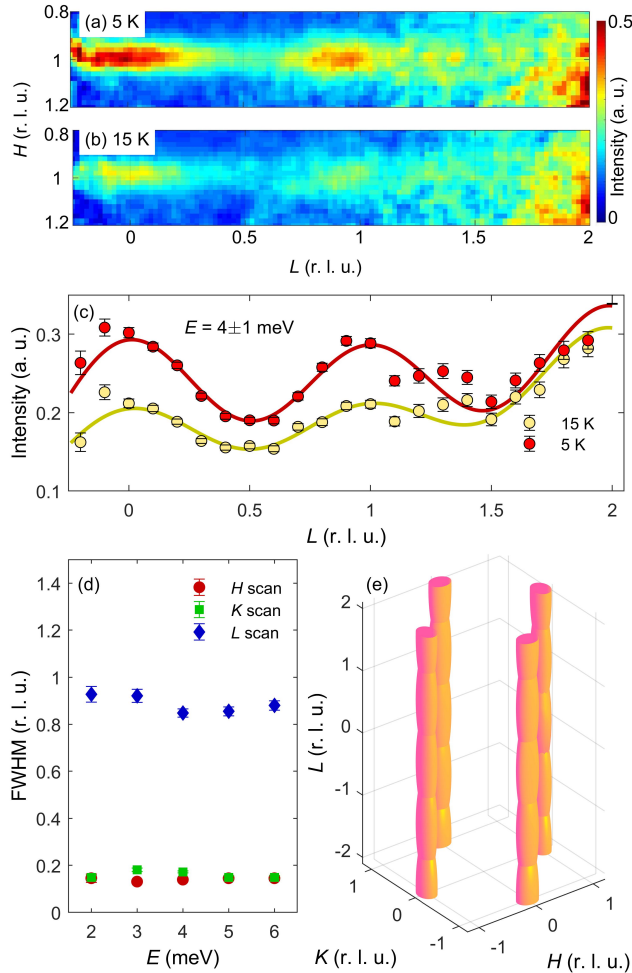


FIG. 4. (a-b) Constant-energy maps of  $\text{FeSe}_{0.93}\text{S}_{0.07}$  obtained at  $T = 5\text{ K}$  and  $15\text{ K}$  and in  $(H, L)$  momentum plane with  $E = 4 \pm 1\text{ meV}$  and  $|K| \leq 0.1$ . (c)  $L$  scans at  $T = 5\text{ K}$  and  $15\text{ K}$  with  $E = 4 \pm 1\text{ meV}$ ,  $|K| \leq 0.1$  and  $|H - 1| \leq 0.1$ . (d) Energy dependence of FWHM for  $H$ ,  $K$  and  $L$  scans fitted by gaussian functions [See Fig. S3 in Supplementary Materials]. (e) The 3D distribution of spin excitation in momentum space using FWHM data from  $E = 4 \pm 1\text{ meV}$ . Solid lines in are Gaussian functions obtained by fitting the respective data.

widths at half maximum (FWHM) value  $\kappa_H$ ,  $\kappa_K$  and  $\kappa_L$  as shown in Fig. 4(d). Comparing the FWHM along  $H$  and  $K$  directions,  $\kappa_H$  and  $\kappa_K$ , respectively, one observes that the latter is slightly larger than the former. With a 6 times larger value  $\kappa_L$  than  $\kappa_K$ , the  $L$  dependence of intensity suggests a much more broadened distribution of spin excitations along  $L$  direction, weakened with increasing energy and persisting up to  $E \approx 15\text{ meV}$  as shown in Fig. S3-S4 [See Supplementary Materials]. According to the FWHM we draw the schematic diagram of three dimensional distribution of spin excitations in momentum space at  $T = 15\text{ K}$  and  $E = 4\text{ meV}$  as displayed in Fig. 4(e). The ellipsoids are periodically located at  $\mathbf{Q} = (\pm 1, 0, L)$  or  $(0, \pm 1, L)$  in a twinned

sample where  $L$  is integer.

We now discuss the implications of our observed INS results. The feature of integer- $L$  intensity enhancement of spin excitations in  $\text{FeSe}_{1-x}\text{S}_x$  still survives in the nematic state persisting up to  $E \approx 15\text{ meV}$  and tells us that the spins in nearest-neighbor  $\text{FeSe}_4$  layers are parallel and fluctuate in phase, which is opposite to the antiferromagnetic order in the parent compound of Fe-pnictides with antiparallel spins of the nearest-neighbor layers along  $c$ -axis. A ferromagnetic-like inter-layer coupling  $\mathbf{J}_\perp$  has to be responsible for the integer- $L$  intensity modulation in  $\text{FeSe}_{1-x}\text{S}_x$ .

The microscopic origin of the absence of the long-range stripe magnetic order in FeSe remains elusive. One scenario is that the stripe magnetic order in FeSe is absent due to the development of other competing instabilities, considering mainly on the in-plane frustrated magnetic interactions [38–42]. From another point of view, a realistic three-dimensional antiferromagnetic order requires both the spin correlations in and out of plane. The FWHM of spin excitations obtained by Gaussian fitting along  $H$ ,  $K$  and  $L$  directions is associated with the spin-spin correlation length  $\xi_a$ ,  $\xi_b$ ,  $\xi_c$ . The FWHM along  $L$  scans is 6 times larger than along the transverse scans as the smaller correlation length  $\xi_c$  is able to capture the reciprocal space broadening along the long axis  $L$ . As it is well established that intercalating between the Fe layers can strengthen superconductivity and reduce inter-layer coupling [18–23], it seems that superconductivity is a more robust phenomenon in the two-dimensional limit compared to antiferromagnetic order.

#### IV. Conclusion

In conclusion, the anisotropic momentum distribution of spin resonance in  $\text{FeSe}_{1-x}\text{S}_x$  mimics the low energy spin excitations in its nematic phase where superconductivity arises, which implies the close relationship between superconductivity and magnetism. The strongly  $L$ -modulated spin resonance mode inherits the low-energy magnetic scattering in nematic state with maximum intensity at integer  $L$ . FeSe does not order antiferromagnetically, which is unusual among Fe-based materials. The ferromagnetic nature of the inter-layer coupling might shed light on the absence of magnetic order in FeSe.

#### Acknowledgement

The work was supported by the National Key Research and Development of China (Grant No. 2018YFA0704200, 2022YFA1602800), the National Natural Science Foundation of China (Grant No. 12004418) and the Strategic

Priority Research Program of Chinese Academy of Sciences (Grant No. XDB25000000). One of the neutron scattering experiments was performed at the MLF, J-PARC, Japan, under a user program (No. 2018A0019).

\* mw\_ma@iphy.ac.cn

† Present address: Clarendon Laboratory, University of Oxford, Parks Road, Oxford OX1 3PU, United Kingdom

‡ yuan.li@pku.edu.cn

- [1] D. J. Scalapino, Rev. Mod. Phys. **84**, 1383 (2012).
- [2] J. M. Tranquada, G. Xu, and I. A. Zaliznyak, Journal of Magnetism and Magnetic Materials **350**, 148 (2014).
- [3] P. Dai, Rev. Mod. Phys. **87**, 855 (2015).
- [4] M. Eschrig, Adv. Phys. **55**, 47 (2006).
- [5] S. Chi, A. Schneidewind, J. Zhao, L. W. Harriger, L. Li, Y. Luo, G. Cao, Z. Xu, M. Loewenhaupt, J. Hu, and P. Dai, Phys. Rev. Lett. **102**, 107006 (2009).
- [6] S. Li, Y. Chen, S. Chang, J. W. Lynn, L. Li, Y. Luo, G. Cao, Z. Xu, and P. Dai, Phys. Rev. B **79**, 174527 (2009).
- [7] D. K. Pratt, A. Kreyssig, S. Nandi, N. Ni, A. Thaler, M. D. Lumsden, W. Tian, J. L. Zarestky, S. L. Bud'ko, P. C. Canfield, A. I. Goldman, and R. J. McQueeney, Phys. Rev. B **81**, 140510 (2010).
- [8] C. Zhang, R. Yu, Y. Su, Y. Song, M. Wang, G. Tan, T. Egami, J. A. Fernandez-Baca, E. Faulhaber, Q. Si, and P. Dai, Phys. Rev. Lett. **111**, 207002 (2013).
- [9] C. Stock, C. Broholm, J. Hudis, H. J. Kang, and C. Petrovic, Phys. Rev. Lett. **100**, 087001 (2008).
- [10] C. H. Lee, P. Steffens, N. Qureshi, M. Nakajima, K. Kihou, A. Iyo, H. Eisaki, and M. Braden, Phys. Rev. Lett. **111**, 167002 (2013).
- [11] H. F. Fong, B. Keimer, D. Reznik, D. L. Milius, and I. A. Aksay, Phys. Rev. B **54**, 6708 (1996).
- [12] J. M. Tranquada, P. M. Gehring, G. Shirane, S. Shamoto, and M. Sato, Phys. Rev. B **46**, 5561 (1992).
- [13] H. Chou, J. M. Tranquada, G. Shirane, T. E. Mason, W. J. L. Buyers, S. Shamoto, and M. Sato, Phys. Rev. B **43**, 5554 (1991).
- [14] S. Pailhès, Y. Sidis, P. Bourges, C. Ulrich, V. Hinkov, L. P. Regnault, A. Ivanov, B. Liang, C. T. Lin, C. Bernhard, and B. Keimer, Phys. Rev. Lett. **91**, 237002 (2003).
- [15] T. Xie, Y. Wei, D. Gong, T. Fennell, U. Stuhr, R. Kajimoto, K. Ikeuchi, S. Li, J. Hu, and H. Luo, Phys. Rev. Lett. **120**, 267003 (2018).
- [16] L. Capogna, B. Fauqué, Y. Sidis, C. Ulrich, P. Bourges, S. Pailhès, A. Ivanov, J. L. Tallon, B. Liang, C. T. Lin, A. I. Rykov, and B. Keimer, Phys. Rev. B **75**, 060502 (2007).
- [17] S. Pailhès, Y. Sidis, P. Bourges, V. Hinkov, A. Ivanov, C. Ulrich, L. P. Regnault, and B. Keimer, Phys. Rev. Lett. **93**, 167001 (2004).
- [18] Y. Qiu, W. Bao, Y. Zhao, C. Broholm, V. Stanev, Z. Tesanovic, Y. C. Gasparovic, S. Chang, J. Hu, B. Qian, M. Fang, and Z. Mao, Phys. Rev. Lett. **103**, 067008 (2009).
- [19] G. Friemel, J. T. Park, T. A. Maier, V. Tsurkan, Y. Li, J. Deisenhofer, H.-A. Krug von Nidda, A. Loidl, A. Ivanov, B. Keimer, and D. S. Inosov, Phys. Rev. B **85**, 140511 (2012).
- [20] M. Ramazanoglu, J. Lamsal, G. S. Tucker, J.-Q. Yan, S. Calder, T. Guidi, T. Perring, R. W. McCallum, T. A. Lograsso, A. Kreyssig, A. I. Goldman, and R. J. McQueeney, Phys. Rev. B **87**, 140509 (2013).
- [21] N. Qureshi, P. Steffens, Y. Drees, A. C. Komarek, D. Lamago, Y. Sidis, L. Harnagea, H.-J. Grafe, S. Wurmehl, B. Büchner, and M. Braden, Phys. Rev. Lett. **108**, 117001 (2012).
- [22] B. Pan, Y. Shen, D. Hu, Y. Feng, J. T. Park, A. D. Christianson, Q. Wang, Y. Hao, Z. Wo, Hongliang Yin, T. A. Maier, and J. Zhao, Nat. Commun. **8**, 123 (2017).
- [23] M. Ma, L. Wang, P. Bourges, Y. Sidis, S. Danilkin, and Y. Li, Phys. Rev. B **95**, 100504 (2017).
- [24] F.-C. Hsu, J.-Y. Luo, K.-W. Yeh, T.-K. Chen, T.-W. Huang, P. M. Wu, Y.-C. Lee, Y.-L. Huang, Y.-Y. Chu, D.-C. Yan, and M.-K. Wu, Proceedings of the National Academy of Sciences **105**, 14262 (2008).
- [25] B. Lei, J. H. Cui, Z. J. Xiang, C. Shang, N. Z. Wang, G. J. Ye, X. G. Luo, T. Wu, Z. Sun, and X. H. Chen, Phys. Rev. Lett. **116**, 077002 (2016).
- [26] B. Lei, N. Z. Wang, C. Shang, F. B. Meng, L. K. Ma, X. G. Luo, T. Wu, Z. Sun, Y. Wang, Z. Jiang, B. H. Mao, Z. Liu, Y. J. Yu, Y. B. Zhang, and X. H. Chen, Phys. Rev. B **95**, 020503 (2017).
- [27] T. P. Ying, M. X. Wang, X. X. Wu, Z. Y. Zhao, Z. Z. Zhang, B. Q. Song, Y. C. Li, B. Lei, Q. Li, Y. Yu, E. J. Cheng, Z. H. An, Y. Zhang, X. Y. Jia, W. Yang, X. H. Chen, and S. Y. Li, Phys. Rev. Lett. **121**, 207003 (2018).
- [28] X. F. Lu, N. Z. Wang, H. Wu, Y. P. Wu, D. Zhao, X. Z. Zeng, X. G. Luo, T. Wu, W. Bao, G. H. Zhang, F. Q. Huang, Q. Z. Huang, and X. H. Chen, Nature Mater. **14**, 325 (2015).
- [29] A. Krzton-Maziopa, E. V. Pomjakushina, V. Y. Pomjakushin, F. von Rohr, A. Schilling, and K. Conder, Journal of Physics: Condensed Matter **24**, 382202 (2012).
- [30] J. Guo, S. Jin, G. Wang, S. Wang, K. Zhu, T. Zhou, M. He, and X. Chen, Phys. Rev. B **82**, 180520 (2010).
- [31] J. Guo, H. Lei, F. Hayashi, and H. Hosono, Nature Commun. **5**, 4756 (2014).
- [32] T. P. Ying, X. L. Chen, G. Wang, S. F. Jin, T. T. Zhou, X. F. Lai, H. Zhang, and W. Y. Wang, Sci. Rep. **2**, 426 (2012).
- [33] Q. Wang, Z. Li, W. Zhang, Z. Zhang, J. Zhang, W. Li, H. Ding, Y. Ou, P. Deng, K. Chang, J. Wen, C. Song, K. He, J. Jia, S. Ji, Y. Wang, L. Wang, X. Chen, X. Ma, and Q. Xue, Chin. Phys. Lett. **29**, 037402 (2012).
- [34] S. He, J. He, W. Zhang, L. Zhao, D. Liu, X. Liu, D. Mou, Y. Ou, Q. Wang, Z. Li, L. Wang, Y. Peng, Y. Liu, C. Chen, L. Yu, G. Liu, X. Dong, J. Zhang, C. Cheng, Z. Xu, X. Chen, X. Ma, Q. Xue, and X. Zhou, Nature Mater. **12**, 605 (2013).
- [35] J. Ge, Z. Lu, C. Liu, C. Gao, D. Qian, Q. Xue, Y. Liu, and J. Jia, Nature Mater. **14**, 285 (2015).
- [36] T. M. McQueen, A. J. Williams, P. W. Stephens, J. Tao, Y. Zhu, V. Ksenofontov, F. Casper, C. Felser, and R. J. Cava, Phys. Rev. Lett. **103**, 057002 (2009).
- [37] S.-H. Baek, D. V. Efremov, J. M. Ok, J. S. Kim, J. van den Brink, and B. Büchner, Nature Mater. **14**, 210 (2015).
- [38] R. Yu and Q. Si, Phys. Rev. Lett. **115**, 116401 (2015).
- [39] F. Wang, S. A. Kivelson, and D.-H. Lee, Nature Phys. **11**, 959 (2015).
- [40] J. K. Glasbrenner, I. I. Mazin, H. O. Jeschke, P. J. Hirschfeld, R. M. Fernandes, and R. Valentí, Nature

- Phys. **11**, 953 (2015).
- [41] A. V. Chubukov, R. M. Fernandes, and J. Schmalian, Phys. Rev. B **91**, 201105 (2015).
- [42] Y. Yamakawa, S. Onari, and H. Kontani, Phys. Rev. X **6**, 021032 (2016).
- [43] H. Li, M.-W. Ma, S.-B. Liu, F. Zhou, and X.-L. Dong, Chinese Physics B **29**, 127404 (2020).
- [44] W. C. Hamilton, Acta Crystallographica **10**, 629 (1957).
- [45] A. I. Coldea, Frontiers in Physics **8** (2021).
- [46] R. Kajimoto, M. Nakamura, Y. Inamura, F. Mizuno, K. Nakajima, S. Ohira-Kawamura, T. Yokoo, T. Nakatani, R. Maruyama, K. Soyama, K. Shibata, K. Suzuya, S. Sato, K. Aizawa, M. Arai, S. Wakimoto, M. Ishikado, S.-i. Shamoto, M. Fujita, H. Hiraka, K. Ohoyama, K. Yamada, and C.-H. Lee, Journal of the Physical Society of Japan **80**, SB025 (2011).
- [47] M. Nakamura, R. Kajimoto, Y. Inamura, F. Mizuno, M. Fujita, T. Yokoo, and M. Arai, Journal of the Physical Society of Japan **78**, 093002 (2009).
- [48] Y. Inamura, T. Nakatani, J. Suzuki, and T. Otomo, Journal of the Physical Society of Japan **82**, SA031 (2013).
- [49] Y. Gu, Q. Wang, H. Wo, Z. He, H. C. Walker, J. T. Park, M. Enderle, A. D. Christianson, W. Wang, and J. Zhao, Phys. Rev. B **106**, L060504 (2022).
- [50] Q. Wang, Y. Shen, B. Pan, Y. Hao, M. Ma, F. Zhou, P. Steffens, K. Schmalzl, T. R. Forrest, M. Abdel-Hafiez, X. Chen, D. A. Chareev, A. N. Vasiliev, P. Bourges, Y. Sidis, H. Cao, and J. Zhao, Nature Mater. **15**, 159 (2016).
- [51] Q. Wang, Y. Shen, B. Pan, X. Zhang, K. Ikeuchi, K. Iida, A. D. Christianson, H. C. Walker, D. T. Adroja, M. Abdel-Hafiez, X. Chen, D. A. Chareev, A. N. Vasiliev, and J. Zhao, Nature Commun. **7**, 12182 (2016).
- [52] M. Ma, P. Bourges, Y. Sidis, Y. Xu, S. Li, B. Hu, J. Li, F. Wang, and Y. Li, Phys. Rev. X **7**, 021025 (2017).
- [53] T. Chen, Y. Chen, A. Kreisel, X. Lu, A. Schneidewind, Y. Qiu, J. T. Park, J. R. Perring, Toby G. and Stewart, H. Cao, R. Zhang, Y. Li, Y. Rong, Y. Wei, B. M. Andersen, P. J. Hirschfeld, C. Broholm, and P. Dai, Nat. Mater. **18**, 709 (2019).
- [54] M. G. Kim, G. S. Tucker, D. K. Pratt, S. Ran, A. Thaler, A. D. Christianson, K. Marty, S. Calder, A. Podlesnyak, S. L. Bud'ko, P. C. Canfield, A. Kreyssig, A. I. Goldman, and R. J. McQueeney, Phys. Rev. Lett. **110**, 177002 (2013).
- [55] M. Ma, P. Bourges, Y. Sidis, A. Ivanov, G. Chen, Z. Ren, and Y. Li, Phys. Rev. B **107**, 184516 (2023).
- [56] D. Hu, Z. Yin, W. Zhang, R. A. Ewings, K. Ikeuchi, M. Nakamura, B. Roessli, Y. Wei, L. Zhao, G. Chen, S. Li, H. Luo, K. Haule, G. Kotliar, and P. Dai, Phys. Rev. B **94**, 094504 (2016).